Next-Generation Lithium Metal Anode Engineering *via* Atomic Layer Deposition

Alexander C. Kozen,[†,‡] Chuan-Fu Lin,[†,‡] Alexander J. Pearse,[†,‡] Marshall A. Schroeder,[†,‡] Xiaogang Han,[†] Liangbing Hu,[†] Sang-Bok Lee,[§] Gary W. Rubloff,[†,‡] and Malachi Noked*[,†,‡,§]

[†]Department of Materials Science & Engineering, [‡]Institute for Systems Research, and [§]Department of Chemistry, University of Maryland College Park, Maryland 20742, United States

ABSTRACT Lithium metal is considered to be the most promising anode for next-generation batteries due to its high energy density of 3840 mAh g^{-1}. However, the extreme reactivity of the Li surface can induce parasitic reactions with solvents, contamination, and shuttled active species in the electrolyte, reducing the performance of batteries employing Li metal anodes. One promising solution to this issue is application of thin chemical protection layers to the Li metal surface. Using a custom-made ultrahigh vacuum integrated deposition and characterization system, we demonstrate atomic layer deposition (ALD) of protection layers directly on Li metal with exquisite thickness control. We demonstrate as a proof-of-concept that a 14 nm thick ALD Al_2O_3 layer can protect the Li surface from corrosion due to atmosphere, sulfur, and electrolyte exposure. Using Li–S battery cells as a test system, we demonstrate an improved capacity retention using ALD-protected anodes over cells assembled with bare Li metal anodes for up to 100 cycles.

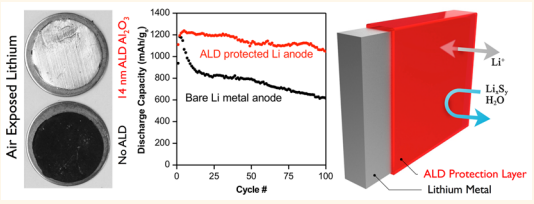

KEYWORDS: atomic layer deposition · solid electrolyte interface · lithium metal anode · lithium protection · lithium–sulfur

The ever-increasing demand for higher energy density storage devices for transportation (electric vehicles), grid storage (power leveling), and other applications is challenging the scientific community to develop a rechargeable battery with a cycle life comparable to that of the Li-ion but with significantly higher capacity. Major R&D centers increasingly look to metal anode systems, including Li–S and Li–O_2, and advanced oxide cathode systems combined with Li metal anodes for increased performance. Recent analysis of beyond-Li-ion options by the Joint Center for Energy Storage Research (JCESR) highlights the high priority for metal anode systems, while recognizing that the reactivity of the metal anode poses serious technical and manufacturing challenges.[1]

From an operational point of view, lithium's high reactivity with most organic chemicals used in battery electrolytes causes corrosion reactions to occur during cycling due to reduction of solvents, active species, or impurities in the electrolyte, eventually leading to degradation of the anode, consumption of electrolyte and active materials, and eventual battery failure.

In fact, the battery industry expended considerable effort to commercialize Li metal anodes *via* electrolyte additive engineering in the late 1980s.[2−4] However, due to the propensity of lithium metal to form dangerous dendrites upon repeated cycling, resulting in a number of high profile fires in 1989, the use of lithium anodes decreased in popularity.[3]

Realization of stable Li metal anodes in rechargeable batteries is a challenge with many facets. From a processing perspective, lithium metal will oxidize and corrode under atmospheric conditions from H_2O and CO_2 exposure *via* the stepwise reactions

$$2Li + 2H_2O \rightarrow 2LiOH + H_2 \quad (1)$$

$$2LiOH + CO_2 \rightarrow Li_2CO_3 + H_2O \quad (2)$$

producing a characteristic black tarnish on the Li metal surface.[5] This oxidation is prevented by limiting the exposure of the Li metal to H_2O, necessitating the use of costly dry rooms for lithium metal extrusion and battery assembly.

Lithium metal protection is particularly important in systems where the active

* Address correspondence to malachi@umd.edu.

Received for review January 21, 2015 and accepted May 13, 2015.

Published online May 13, 2015
10.1021/acsnano.5b02166

material diffuses freely through the electrolyte (*e.g.*, polysulfide in Li−S cells) or if inherent contamination is present in the electrolyte (*e.g.*, H_2O, CO_2, and N_2 in a real Li−air system). In both of these cases, the highly reactive Li anode forms a high impedance solid electrolyte interphase layer on its surface, consuming electrolyte and active material, resulting in practical capacity loss and low Coulombic efficiency.[6]

Previous attempts to passivate Li metal with organic molecules[7,8] and polymeric coatings[9,10] have achieved limited success due to poor thickness and compositional control of the applied protection layer. Protection with sputtered solid electrolytes,[11,12] while effective at preventing electrolyte decomposition on the Li metal surface, can result in large cell overpotentials during recharge at even moderate rates due to the large thicknesses (~micrometers) and low ionic conductivity of the sputtered solid electrolytes. Recently, protection of the Li surface with self-assembled carbon spheres[13] has proven to be effective at preventing Li dendrite growth upon cycling but offers limited options for scalable manufacturing and also adds significant mass to the anode. Lithium metal powder is commercially available from the FMC company and shows promise toward stable lithium anodes.[7,14]

We suggest a new approach to study Li metal surface stabilization *via* application of atomic layer deposition (ALD) protection layers directly on the Li metal, creating a new thin phase between the metal and various corrosive surroundings. Using a unique ultrahigh vacuum (UHV) system described elsewhere,[15] we deposited ALD Al_2O_3 coatings directly on Li metal foil to mitigate corrosion reactions due to both atmosphere and electrolyte exposure. We determine and measure directly, for the first time, the nominal layer thickness for effective Li metal protection, and we use Li−S cells to demonstrate a dramatic capacity increase of protected Li metal anodes over their unprotected counterparts *via* mitigation of the Li corrosion by sulfur species shuttling in the electrolyte.[16] While the focus of this work is on Li metal anodes, our study opens a new opportunity for realization of other metal-anode-based systems such as Na and Mg rechargeable batteries and for protection of those metal by various thin layers deposited atomically or molecularly.

RESULTS AND DISCUSSION

Deposition of ALD Protection Coatings on Lithium Metal Anodes. ALD is ideally suited to Li metal protection due to its unique properties of angstrom-scale thickness control, pinhole-free conformal films, and low-temperature deposition below the melting point of lithium (180 °C).[17] ALD coatings have proven to be effective passivation layers for metals such as Cu,[18] Mg,[19] and steel[20] from corrosion in electrolytes and effective water vapor transmission barriers on polymers[21] and even reactive metals such as Ca.[22] In batteries, thin ALD coatings have been applied to nonmetallic anodes[23−26] and cathodes[27−29] to improve battery cycling performance; however, to maintain high ionic conductivities without increasing cell impedance, these ALD coatings are less than 2 nm thick. In contrast to these previous studies, we find that <2 nm ALD coatings are not of sufficient thickness for Li metal protection.

In this work, we focus exclusively on ALD Al_2O_3 protection layers, due to the ideal ALD process chemistry that can coat Li metal and the known lithiation mechanism of Al_2O_3 to form the stable, ionically conductive $Li_xAl_2O_3$ alloy.[30] While the surface of the Li metal is covered with a native oxide as seen in the Li 1s photoelectron peak in Figure 1A, this peak is extinguished after application of a 14 nm thick ALD protective layer as shown in Figure 1C, which only contains photoelectron peaks consistent with Al_2O_3. Figure 1B shows 5 nm ALD Al_2O_3 directly on Li metal, which exhibits characteristic photoelectron peaks of both Al_2O_3 and Li metal. At 14 nm, the ALD layer is thicker than the escape depth of the photoelectrons; therefore, a lack of a Li 1s peak after application of the Al_2O_3 layer indicates not only that the ALD coating is uniform and pinhole-free but also that the top ~8 nm of the layer does not lithiate during the ALD process at 100 °C. X-ray photoelectron spectra (XPS) of thinner ALD layers on Li metal do exhibit the Li 1s photoelectron peak, indicating that these films either are thinner than the escape depth of the photoelectrons from the underlying Li metal or may contain pinhole defects.

Lithium Corrosion Prevention in Three Environments. We take a stepwise approach to testing the effectiveness

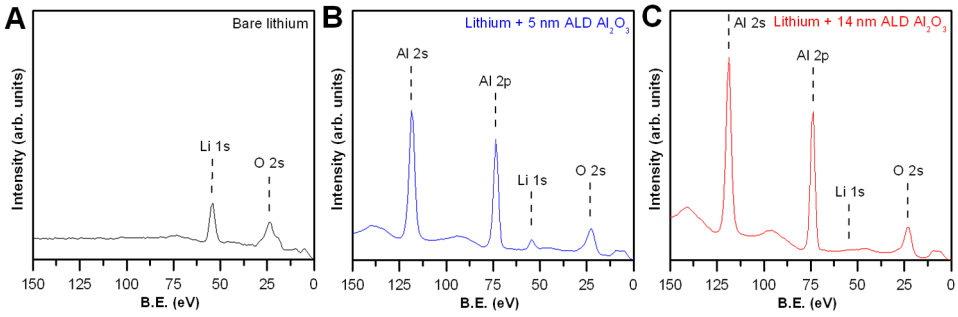

Figure 1. XPS of (A) uncycled pristine Li metal; (B) uncycled Li metal protected with 5 nm ALD Al_2O_3; (C) uncycled Li metal protected with 14 nm ALD Al_2O_3.

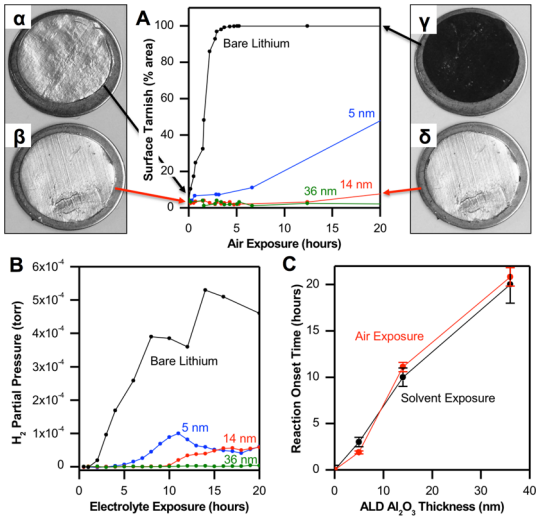

Figure 2. (A) Optical analysis of lithium foil surface tarnishing during atmospheric exposure at 25 °C and 40% RH. (B) Evolution of H_2 gas during organic solvent exposure. (C) Correlation between onset time for atmospheric tarnishing and onset time for H_2 evolution (see Methods for tarnish quantification by ImageJ). (α) Unprotected and (β) 14 nm ALD Al_2O_3-protected Li metal foil immediately upon removal from an argon atmosphere. (γ) Bare and (δ) 14 nm ALD Al_2O_3-protected Li metal foil after 20 h exposed to atmosphere at 25 °C and 40% RH.

of our ALD protection layers on Li metal surfaces, with the intent of simulating three environments where opportunities for contamination and subsequent chemical corrosion occur during either Li metal processing, battery assembly and storage, and finally battery operation.

Atmospheric Corrosion. To test the effect of ALD protection layers against atmospheric corrosion of Li metal by H_2O and CO_2, we exposed pristine and ALD Al_2O_3-protected Li metal foil to a controlled laboratory environment of 25 °C and 40% RH. We took periodic photographs of the Li metal surface under controlled lighting and camera conditions, and then used ImageJ to calculate the amount of surface corrosion that had occurred. Figure 2A tracks the percent of Li surface tarnishing as a function of air exposure time. Notably, unprotected lithium metal begins tarnishing almost immediately after air exposure (<1 min), while lithium foils coated with 14 nm ALD Al_2O_3 can prevent the onset of surface tarnishing by 20 h, with higher thicknesses both delaying the onset of measurable surface tarnishing as well as hindering the tarnishing rate once it begins.

Organic Solvent Corrosion. As a test case for the efficacy of ALD protection layers at preventing decomposition due to reactions with organic solvents, we immersed bare and protected Li in propylene carbonate (PC). By using differential quadrupole mass spectroscopy (dQMS), we sampled the gaseous byproducts that evolved during the reaction of ALD Al_2O_3-protected and unprotected Li metal with PC. PC was chosen because it has a known high reactivity with Li surfaces;[31] indeed, the autodecomposition of PC has been studied as a protection agent of Li surfaces for Li–air batteries.[32] Second, PC has a low vapor pressure, making it suitable for mass spectroscopy headspace sampling without appreciable loss of electrolyte volume over long periods of time (*e.g.*, days). Our approach enables quantitative detection of the gas phase products that evolved due to surface reaction of the electrolyte on the interface of bare and protected metallic Li; however, for the purposes of this study, we only measure the evolved H_2 gas from these solutions, as H_2 gas is a viable indicator of multiple Li metal corrosion and electrolyte decomposition reactions.

In Figure 2B, we plot the H_2 partial pressure in the container headspace as a function of time for various Al_2O_3 protection layer thicknesses. Hydrogen evolution from Li metal anodes is a well-known indicator of corrosion reactions.[33] The onset time for H_2 evolution is linearly proportional to the thickness of the ALD layer, indicating that contamination is diffusing through the ALD layer to the Li metal. Additionally, after onset of H_2 evolution, the H_2 partial pressure in the headspace above the ALD-protected Li is 1 order of magnitude lower than that of the bare Li, indicating that ALD protection also reduces the extent of anode degradation *via* parasitic reactions with the electrolyte. This is in good agreement with what we found with the air exposure, as the ALD protection layer is both delaying corrosion and hindering the corrosion reaction once it begins. We attribute that to a self-healing mechanism in which ALD protection layers <15 nm contain defects which localize electrolyte decomposition reactions; however, once a stable phase is formed at these defect sites, the corrosion reaction is diminished to match that of the fully protected Li metal.

Both of these experiments demonstrating direct comparison of the reactivity of pristine and protected Li metal allow us to extract a relationship between protection layer thickness and degree of lithium protection, as shown in Figure 2C. Remarkably, we find ALD Al_2O_3 has an effective protection thickness dependence of approximately 1.8 h/nm, independent of atmosphere or liquid exposure environment, suggesting that the duration of Li metal protection can be anticipated by careful tailoring of the ALD protection layer thickness.

Dramatic photographic evidence of this protection is exhibited *via* the remarkable optical differences in the lithium surface between unprotected and protected Li metal upon initial air exposure (Figure 2α,β, respectively) and after 20 h of air exposure (Figure 2γ,δ, respectively) at 25 °C and 40% RH.

Sulfur and DME Corrosion. We tested the efficacy of our protection layer on the Li surface by soaking it in a solution of dimethyoxylane (DME) and elemental sulfur to simulate a fully assembled Li–S battery in storage.

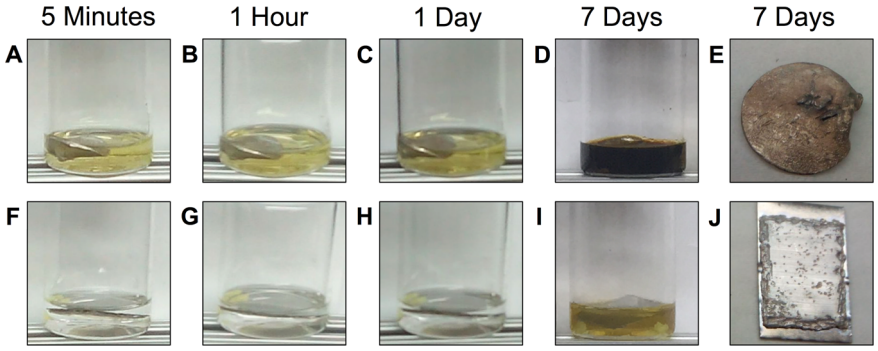

Figure 3. Optical images of (A–E) unprotected and (F–J) 14 nm ALD Al_2O_3-protected Li metal foil soaked in 1 M sulfur/DME solution for 7 days.

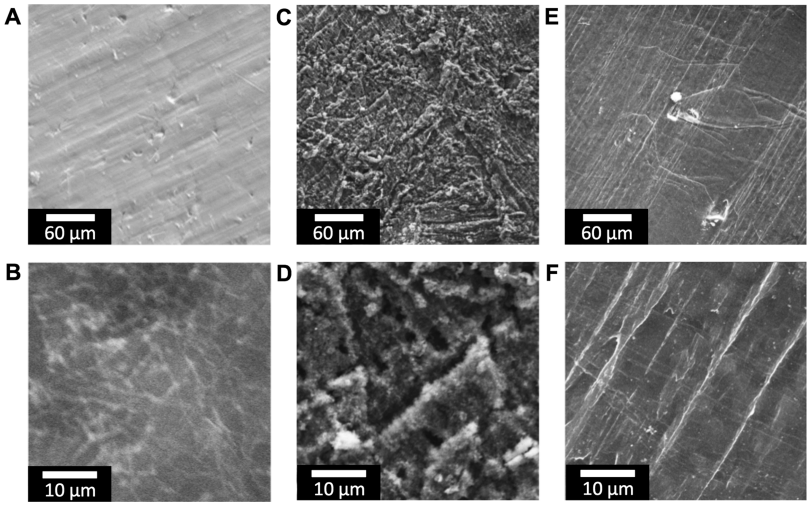

Figure 4. SEM images of (A,B) unprotected Li metal before solvent exposure. (C,D) Unprotected Li metal after 7 days of exposure to DME/sulfur solution and (E,F) 14 nm ALD Al_2O_3-protected Li metal surface after 7 days of exposure to DME/sulfur solution.

Although the solubility of elemental sulfur from the cathode in glyme electrolytes (commonly used for Li–S batteries) is relatively low, it can still allow enough sulfur in the electrolyte to induce Li anode corrosion. First, long-chain soluble Li polysulfides (PS) are formed, changing the visual appearance of the DME solvent from clear to yellow-brown. This effect is shown in Figure 3, where bare Li metal readily forms PS in solution, while 14 nm ALD Al_2O_3-protected Li metal soaked in the same solution demonstrates remarkable stability against spontaneous PS formation.

Once long-chain PS are formed in the organic solvent solution, these PS are further reduced into short-chain PS and precipitate as insulating Li_2S on the Li anode surface. Bare and protected Li metal soaked in DME/S for 7 days and then washed with pure DME are shown in Figure 3. Clearly, there is significant PS deposition on the bare Li metal surface, while the ALD-protected metal surface exhibits improved stability and appears optically similar to the unreacted Li metal surface. Scanning electron microscopy (SEM) images of these surfaces are shown in Figure 4, which, in the case of bare Li metal, exhibit major morphological changes, while the ALD-protected Li metal surface remains intact and relatively unchanged. This effect may cause Li corrosion even when the battery cell is resting before the start of cycling and drastically reduces the performance of Li–S cells after manufacture before the battery is placed into service by consuming available sulfur from the cathode into non-electrochemically active species.

Lithiation Behavior of the Protected Anode. Figure 5 shows the cyclic voltammogram (CV) and impedance responses for both unprotected and 14 nm Al_2O_3-protected lithium metal working electrodes cycled between −1 and 1.1 V *vs* Li in a Tee-cell configuration to strip and replate Li from the working electrode in order to test the influence of the protection layers on the faradaic processes on the anode surface. The cathodic scan in Figure 5A on the protected electrode shows two different domains with two different slopes for Li plating, whereas the cathodic scan of the bare Li metal in Figure 5C exhibits only one line with an identical slope. After the first three CV cycles, the plating and stripping behavior of both anodes is identical (Figure 5A, inset). We attribute the dual-slope

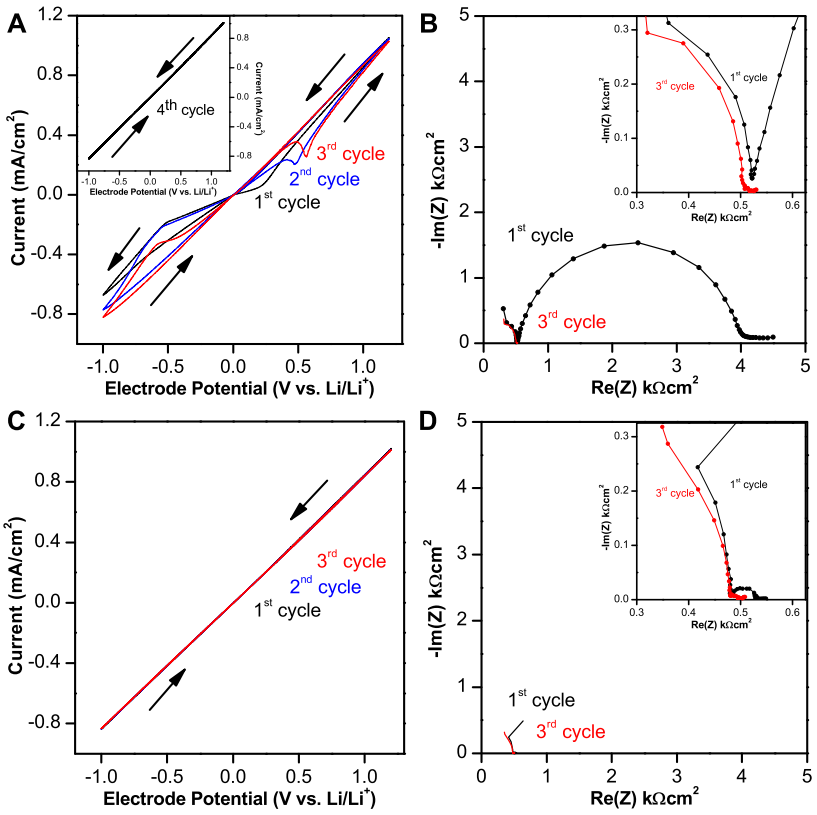

Figure 5. (A) Plot of the first three CV cycles of a lithium metal anode protected with 14 nm ALD Al_2O_3. Inset: Fourth CV cycle. (B) Nyquist plot showing electrochemical impedance spectroscopy (EIS) of the same protected lithium metal anode after the first (black) and third (red) CV cycles. Inset: Expanded region to illustrate high-frequency region of the EIS plot in (B). (C) Plot of the first three CV cycles of a bare lithium metal anode. (D) Nyquist plot showing EIS of the same bare lithium metal anode after the first (black) and third (red) CV cycles. Inset: Expanded region to illustrate high-frequency region of the EIS plot in (D).

behavior of the protected Li CV to a changing impedance for Li plating that resulted from an initial lithiation of the Al_2O_3 layer followed by a subsequent impedance decrease at lower potentials after further lithiation of the Al_2O_3 (Figure 5B,D). For the anodic scan regions, similar lithiation behavior was achieved and maintained for the first three cycles, while again after the first three CV scans, the protected anode exhibits behavior identical to that of the bare Li anode.

While the CV study of the protected and unprotected Li anodes shown in Figure 5 represents the behavior of the Li/Al_2O_3 interface during a potential sweep, the Li anode does not experience a voltage shift of 1.2 V *vs* Li/Li^+ in a real battery. Instead, the Li anode responds to relatively small shifts of the anode voltage by supplying compensation current. Therefore, we also tested the effect of the 14 nm Al_2O_3 layer on the overpotential of the Li anode during galvanostatic (GV) cycling of symmetric cells. Overpotential and impedance spectra (EIS Nyquist plots) of symmetric cells composed of two bare Li electrodes and a symmetric cell composed of two protected Li electrodes shown in Figure 6 demonstrate that the overpotential increase upon application of 0.1 mA cm^{-2} is minimal. This behavior is consistent with previously reported lithium plating studies, and in fact, we find that the influence of the thin ALD Al_2O_3 on the EIS response is similar to the recently published effect of aging the battery in the electrolyte before cycling.[34] It is important to note that the increase in impedance of a full cell will be half the impedance presented in Figure 6, as both sides of our symmetric cell are protected with identical 14 nm thick ALD Al_2O_3 layers. In a full Li–S device, slow Li^+ kinetics of the sulfur-based cathode will dominate the cell impedance, especially in the case of a metal anode.

Lithium–Sulfur Battery Testing. We assembled Li–S CR2032 coin cells with activated carbon cloth (ACC)/sulfur composite cathodes, a previously demonstrated Li–S system with adequate behavior suitable as a proof-of-concept platform to test the efficacy of our anode passivation procedure.[35–37]

The long-term cycling performance of these cells is shown in Figure 7. In the case of the bare Li anode, the lowered capacity of the first cycle strongly suggests a self-discharge mechanism similar to that suggested by Cairns *et al.*,[38] an often downplayed phenomenon in work focusing on Li–S cathode performance. This self-discharge mechanism reduces dissolved sulfur species to polysulfides on the anode surface even before the start of cycling, proceeding as a self-propagating reaction since the medium-chain polysulfides can shuttle

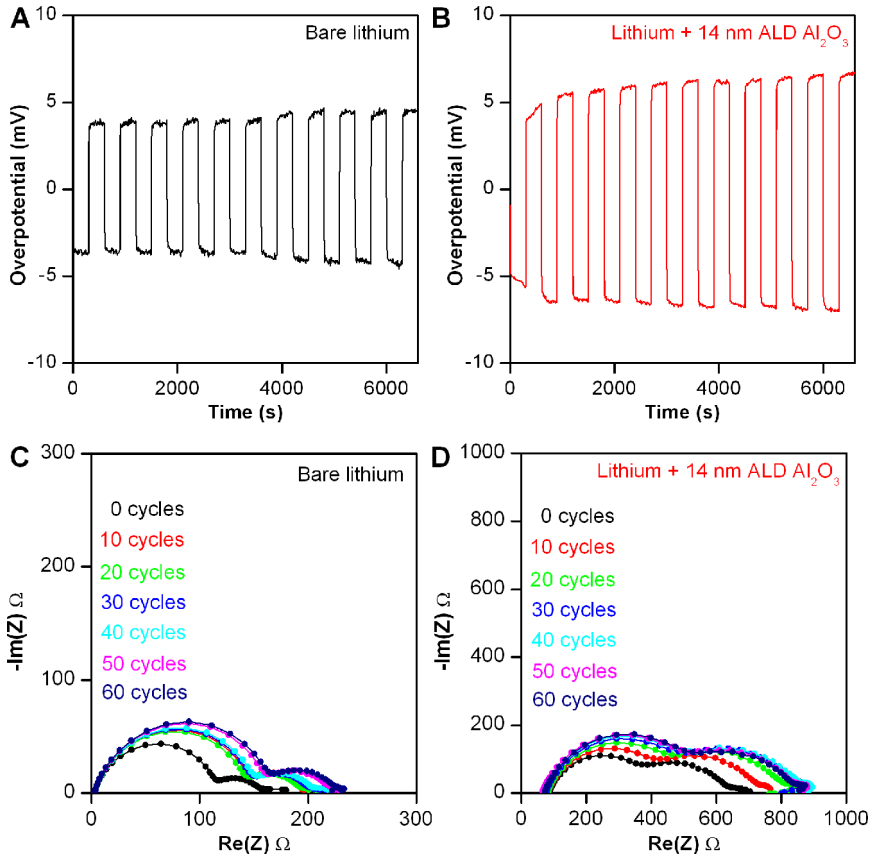

Figure 6. First 10 GV cycles of a symmetric coin cell with (A) two bare lithium metal current collectors and (B) two lithium metal electrodes protected with 14 nm ALD Al_2O_3 showing the overpotential evolution during lithium plating and stripping. (C) EIS response (Nyquist plot) of the symmetric bare lithium metal coin cell before cycling and then subsequently after every 10 GV cycles. (D) Nyquist plot of the symmetric 14 nm ALD Al_2O_3-protected lithium metal coin cell before cycling and then subsequently after every 10 GV cycles.

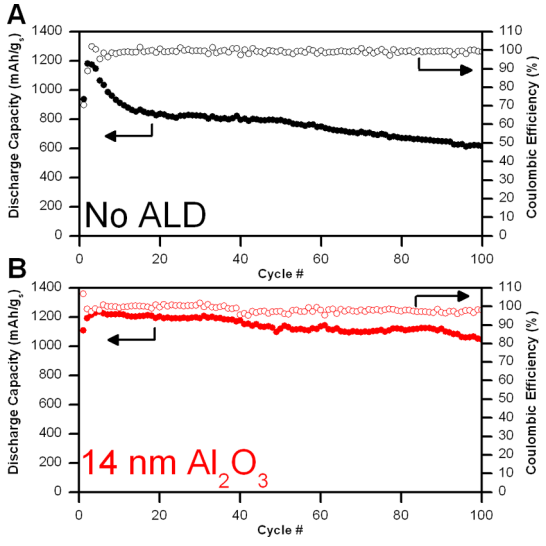

Figure 7. Discharge capacity normalized to sulfur mass (solid circles, left axis) and Coulombic efficiency (open circles, right axis) of both (A) bare Li metal anode and (B) anode protected with 14 nm ALD Al_2O_3 Li–S cells.

back to the cathode and reduce sulfur to long-chain polysulfide. This phenomenon will result in an initial decrease in cell capacity in the first cycle, and as available sulfur is consumed at the anode upon cycling, it will reduce the capacity even further.[10,37] In our case, reactions at the surface of the bare Li metal anode reduce the cell capacity from ~1200 to ~800 mAh g^{-1} after the first 10 cycles, as shown in Figure 7A.

Protection of the Li metal with ALD Al_2O_3 not only prevents this self-discharge during the rest period before we begin electrochemical cycling but also prevents the capacity loss during the first 10 cycles, with the capacity of cells using ALD-protected anodes falling a negligible amount from ~1200 mAh g^{-1} as shown in Figure 7B. This is reinforced by the Coulombic efficiency (CE) of the first two cycles being >95% in the case of the ALD-protected Li and the CE of the first two cycles being 70% and 88% for the bare Li. However, as we are using an excess of Li in our cells, the CE may, in this case, be a less relevant metric as CE is normally associated with cathode degradation.

After 100 cycles, Li–S cells with bare Li metal anodes have lost nearly 50% of their initial capacity, while those with ALD-protected Li metal anodes have lost only ~10% of their initial capacity. Clearly, the ALD Al_2O_3 protection layer increased both initial and long-term capacity of the cell *via* improved utilization of the sulfur by preventing Li metal anode corrosion and thus

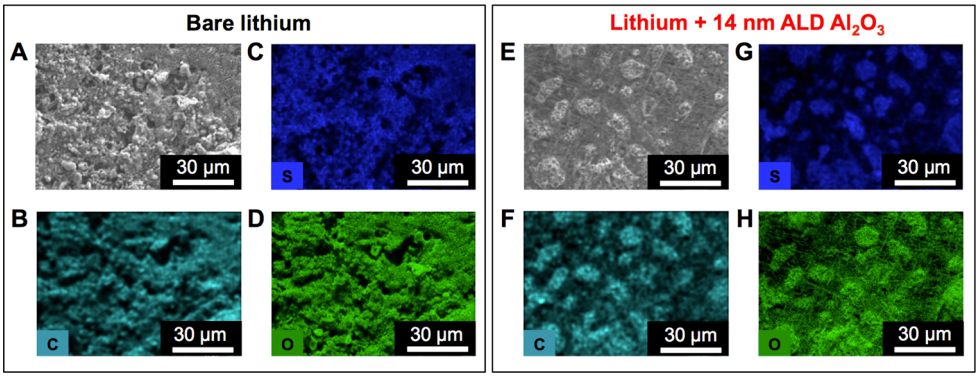

Figure 8. (A) SEM and (B–D) EDX maps of a bare Li metal anode after 100 charge–discharge cycles in a Li–S cell. (E) SEM and (F–H) EDX maps of a 14 nm ALD Al_2O_3-protected Li metal anode after 100 charge–discharge cycles in a Li–S cell.

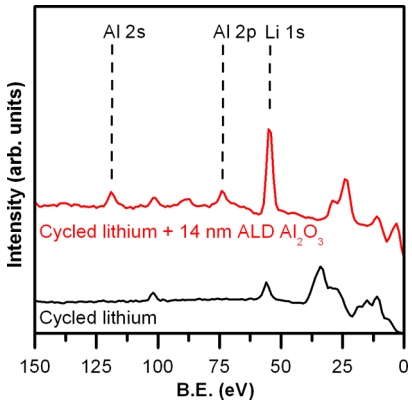

Figure 9. XPS survey spectra of both pristine Li metal and Li metal protected with 14 nm ALD Al_2O_3 after 100 charge–discharge cycles.

enabling cycling with enhanced capacity for up to 100 charge–discharge cycles.

To investigate the extreme situation of sulfur corrosion behavior of the anodes, we cycled a Li–S coin cells with ~5 mg cm^{-2} sulfur and no addition of $LiNO_3$ for 100 charge–discharge cycles (Supporting Information). We disassembled these cells in our glovebox, then washed them with DME to remove excess dried salt, and transferred it to our XPS without subsequent air exposure.

Energy-dispersive X-ray (EDX) images obtained of the Li surface after cycling, shown in Figure 8, show that the density of the sulfur, carbon, and oxygen particulates on the surface of the ALD-protected anode is significantly lower than that on the unprotected anode. Although we do not thoroughly address the morphology of these deposits, their composition and growth conditions suggest hindered dendrite formation on the protected anode surface upon cycling. Due to the low EDX signal from the Al, we are unable to make any conclusions about the state of the ALD film and thus do not include it here. Furthermore, XPS analysis of both the coated and uncoated cycled Li metal surface, shown in Figure 9, indicates that Al_2O_3 remains on the surface of the Li metal after cycling. We attribute this to reduced reactivity of the solvent at the protected metal anode interface *via* prevention of electron transfer from the Li metal to the electrolyte, in general agreement with prior theoretical predictions.[39,40]

CONCLUSIONS

ALD coatings applied directly to Li metal foil could be integrated into the battery fabrication process, particularly given recent advances in atmospheric pressure and low-temperature roll-to-roll ALD tooling.[41] Protecting Li anodes in this way could potentially enable relaxed environmental controls during Li foil manufacture and battery assembly in dry rooms, thus reducing costly overhead during the manufacture of battery materials.

We demonstrate a proof-of-principle for the protection of metallic lithium anodes by application of ALD coatings directly on Li metal. These coatings serve as effective protection barriers against Li metal corrosion upon air, sulfur, and organic solvent exposure. Furthermore, we demonstrate that Li metal protected with only 14 nm ALD Al_2O_3 can drastically reduce first cycle capacity loss in the Li–S system due to prevention of anode corrosion in the presence of sulfur species in the electrolyte. Together, these results clearly demonstrate that ALD is an effective method for protecting Li metal anodes. The versatility of known ALD chemistries provides further options for the composition and functionality of the protection layers. Finally, it seems likely that corresponding benefits can be accessed for other reactive metal anode systems, such as Na, Mg, and Al.

METHODS

Lithium Metal Protection. We stamped disks of Li from 750 μm thick (Alfa Aesar) lithium metal ribbon using a punch and pressed the disks of Li onto stainless steel metal disks for handling. We then transferred the lithium metal to a Cambridge Nanotech Fiji F200 ALD tool also directly connected to the UHV

transfer chamber. Precursors used for the ALD process were trimethylaluminum (TMA, Aldrich, 97%) and plasma O_2, and the reactor temperature was 150 °C. The ALD process used a 0.06 s/30 s/10 s/5 s TMA pulse/purge/$^P O_2$pulse/purge sequence with a growth rate of 1.2 A/cycle. Thickness of the deposited layer was determined by ellipsometric measurements of a blank Si wafer from the same ALD batch using a Cauchy optical model.

Cathode Sulfur Impregnation. Cathodes were fabricated by impregnation of activated carbon cloth with sulfur under vacuum at 150 °C until our desired loading amount was obtained.

Battery Testing. We tested CR2032 coin cells using our anodes and ACC/S cathodes with 0.1 M LiTFSI in 1:1 DME/DOL with 1% $LiNO_3$ electrolyte. For extended cycling, we used Li−S cells loaded with 1.2 and 5 mg cm^{-2} of sulfur and obtained a corresponding capacity of 1.4 and 4 mAh cm^{-2}. The cells were cycled at 0.14 and 0.31 mA cm^{-2} between potential limits of 1.7 and 2.6 V with a rest period of 60 h before the start of cycling. No $LiNO_3$ was used in the sulfur cells for XPS characterization, and the cells were loaded with 5 mg of sulfur per coin cell. Electrochemical cycling was done using an Arbin potentiostat with constant current. CV and EIS measurements were carried out using a Bio-Logic VSP potentiostat in a three-electrode Tee-cell configuration with Li metal as both reference and working electrodes.

Optical Image Analysis. Samples were placed in a controlled laboratory atmosphere at 25 °C and 40% R.H. and imaged using an 8 megapixel Apple iPhone 5 camera from a fixed position under constant lighting conditions. We determined the degree of surface tarnishing using the open source software ImageJ to first convert the images to 8 bit black and white files, to normalize the dynamic range of each pixel from 0 to 255 saturation, and finally to calculate the brightness of each pixel within the lithium metal surface area using binary pixel binning to categorize individual pixels as either nontarnished or tarnished (0−127 or 128−255 saturation, respectively).

Mass Spectroscopy Sampling. Samples were placed into sealed glass vials with 2 mL of 1 M $LiClO_4$ in PC solution at 25 °C. We used a differentially pumped quadrupole mass spectroscopy tool (MKS, Microvision2) to sample the evolved gases in the headspace of the sample containers.

Electrochemistry. We cycled coated and uncoated Li in Swagelok Tee-cells with 0.1 M LiTFSI in 1:1 DME/DOL electrolyte using bare Li metal as both reference and working electrodes. Working electrodes were loaded into the Tee-cell such that the working electrodes were only placed into contact with electrolyte.

XPS. We transferred Li metal from our ALD system directly to an Ar glovebox and then directly to a Kratos Ultra DLD XPS system. XPS spectra were collected using a monochromatic Al Kα source in hybrid lens mode with 160 eV pass energy and 0.1 eV resolution.

Conflict of Interest: The authors declare no competing financial interest.

Supporting Information Available: Optical images of surface tarnishing of Li metal and charge−discharge profiles of both protected and unprotected Li−S batteries with different loading amounts of sulfur. The Supporting Information is available free of charge on the ACS Publications website at DOI: 10.1021/acsnano.5b02166.

Acknowledgment. This work was supported as part of the Nanostructures for Electrical Energy Storage (NEES), an Energy Frontier Research Center funded by the U.S. Department of Energy, Office of Science, Basic Energy Sciences, under Award Number DESC0001160. We acknowledge the support of the Maryland Nanocenter and its NispLab. M.N. acknowledges a postdoctoral fellowship through the Fulbright Program. A.K., M.N., C.L., S.L, and G.R. conceived and designed the experiments. A.K., M.N., C.L., and X.H. performed the experiments. A.K., M.N., and C.L. analyzed the data. M.S., X.H., and A.P. contributed analysis tools. A.K. and M.N. co-wrote the paper.

REFERENCES AND NOTES

1. Gallagher, K. G.; Goebel, S.; Greszler, T.; Mathias, M.; Oelerich, W.; Eroglu, D.; Srinivasan, V. Quantifying the Promise of Lithium−Air Batteries for Electric Vehicles. *Energy Environ. Sci.* **2014**, *7*, 1555.
2. Dan, P.; Mengeritski, E.; Geronov, Y.; Aurbach, D. Performances and Safety Behaviour of Rechargeable AA-Size Li/Li X MnO_2 Cell. *J. Power Sources* **1995**, *54*, 143–145.
3. Xu, K. Nonaqueous Liquid Electrolytes for Lithium-Based Rechargeable Batteries. *Chem. Rev.* **2004**, *104*, 1–116.
4. Mao, H. Polymerizable Aromatic Additives for Overcharge Protection in Non-Aqueous Rechargeable Lithium Batteries. U.S. Patent Appl. US5879834 A, 1999.
5. Arora, P.; White, R. Capacity Fade Mechanisms and Side Reactionsin Lithium-Ion Bateries. *J. Electrochem. Soc.* **1998**, *145*, 3647–3667.
6. Wujcik, K. H.; Velasco-Velez, J.; Wu, C. H.; Pascal, T.; Teran, A. A.; Marcus, M. A.; Cabana, J.; Guo, J.; Prendergast, D.; Salmeron, M.; et al. Fingerprinting Lithium−Sulfur Battery Reaction Products by X-ray Absorption Spectroscopy. *J. Electrochem. Soc.* **2014**, *161*, A1100–A1106.
7. Heine, J.; Krüger, S.; Hartnig, C.; Wietelmann, U.; Winter, M.; Bieker, P. Coated Lithium Powder (CLiP) Electrodes for Lithium-Metal Batteries. *Adv. Energy Mater.* **2013**, 1–7.
8. Marchioni, F.; Star, K.; Menke, E.; Buffeteau, T.; Servant, L.; Dunn, B.; Wudl, F. Protection of Lithium Metal Surfaces Using Chlorosilanes. *Langmuir* **2007**, *23*, 11597–11602.
9. Choi, S. M.; Kang, I. S.; Sun, Y.-K.; Song, J.-H.; Chung, S.-M.; Kim, D.-W. Cycling Characteristics of Lithium Metal Batteries Assembled with a Surface Modified Lithium Electrode. *J. Power Sources* **2013**, *244*, 363–368.
10. Wu, F.; Qian, J.; Chen, R.; Lu, J.; LI, L.; Wu, H.; Chen, J.; Zhao, T.; Ye, Y.; Amine, K. An Effective Approach To Protect Lithium Anode and Improve Cycle Performance for Li−S Batteries. *ACS Appl. Mater. Interfaces* **2014**, 15542–15549.
11. Chung, K.-I.; Kim, W.-S.; Choi, Y.-K. Lithium Phosphorous Oxynitride as a Passive Layer for Anodes in Lithium Secondary Batteries. *J. Electroanal. Chem.* **2004**, *566*, 263–267.
12. Dudney, N. J. Addition of a Thin-Film Inorganic Solid Electrolyte (Lipon) as a Protective Film in Lithium Batteries with a Liquid Electrolyte. *J. Power Sources* **2000**, *89*, 176–179.
13. Zheng, G.; Lee, S. W.; Liang, Z.; Lee, H.-W.; Yan, K.; Yao, H.; Wang, H.; Li, W.; Chu, S.; Cui, Y. Interconnected Hollow Carbon Nanospheres for Stable Lithium Metal Anodes. *Nat. Nanotechnol.* **2014**, *9*, 618–623.
14. Li, Y.; Fitch, B. Effective Enhancement of Lithium-Ion Battery Performance Using SLMP. *Electrochem. Commun.* **2011**, *13*, 664–667.
15. Kozen, A. C.; Schroeder, M. A.; Osborn, K. D.; Lobb, C. J.; Rubloff, G. W. Examining the Role of Hydrogen in the Electrical Performance of *In Situ* Fabricated Metal−Insulator−Metal Trilayers Using an Atomic Layer Deposited Al_2O_3 Dielectric. *Appl. Phys. Lett.* **2013**, *102*, 173501.
16. Yamin, H.; Gorenshtein, A.; Penciner, J.; Sternberg, Y.; Peled, E. Lithium Sulfur Battery Oxidation/Reduction Mechanisms of Polysulfides in THF Solutions. *J. Electrochem. Soc.* **1988**, *135*, 1045–1048.
17. George, S. M. Atomic Layer Deposition: An Overview. *Chem. Rev.* **2010**, *110*, 111–131.
18. Abdulagatov, A. I.; Yan, Y.; Cooper, J. R.; Zhang, Y.; Gibbs, Z. M.; Cavanagh, A. S.; Yang, R. G.; Lee, Y. C.; George, S. M. Al_2O_3 and TiO_2 Atomic Layer Deposition on Copper for Water Corrosion Resistance. *ACS Appl. Mater. Interfaces* **2011**, *3*, 4593–4601.
19. Wang, P. C.; Shih, Y. T.; Lin, M. C.; Lin, H. C.; Chen, M. J.; Lin, K. M. A Study of Atomic Layer Deposited $LiAl_xO_y$ Films on Mg−Li Alloys. *Thin Solid Films* **2010**, *518*, 7501–7504.
20. Marin, E.; Guzman, L.; Lanzutti, A.; Ensinger, W.; Fedrizzi, L. Multilayer Al_2O_3/TiO_2 Atomic Layer Deposition Coatings for the Corrosion Protection of Stainless Steel. *Thin Solid Films* **2012**, *522*, 283–288.
21. Park, M.; Oh, S.; Kim, H.; Jung, D.; Choi, D.; Park, J.-S. Gas Diffusion Barrier Characteristics of Al_2O_3/Alucone Films Formed Using Trimethylaluminum, Water and Ethylene

Glycol for Organic Light Emitting Diode Encapsulation. *Thin Solid Films* **2013**, *546*, 153–156.
22. Bertrand, J. A.; George, S. M. Evaluating Al_2O_3 Gas Diffusion Barriers Grown Directly on Ca Films Using Atomic Layer Deposition Techniques. *J. Vac. Sci. Technol., A* **2013**, *31*, 01A122.
23. Xu, W.; Vegunta, S. S. S.; Flake, J. C. Surface-Modified Silicon Nanowire Anodes for Lithium-Ion Batteries. *J. Power Sources* **2011**, *196*, 8583–8589.
24. Memarzadeh Lotfabad, E.; Kalisvaart, P.; Cui, K.; Kohandehghan, A.; Kupsta, M.; Olsen, B.; Mitlin, D. ALD TiO_2 Coated Silicon Nanowires for Lithium Ion Battery Anodes with Enhanced Cycling Stability and Coulombic Efficiency. *Phys. Chem. Chem. Phys.* **2013**, *15*, 13646.
25. Riley, L.; Cavanagh, A.; George, S.; Lee, S.; Dillon, A. Improved Mechanical Integrity of ALD-Coated Composite Electrodes for Li-Ion Batteries. *Electrochem. Solid-State Lett.* **2011**, *14*, A29.
26. Riley, L. A.; Cavanagh, A. S.; Cavanagh, A. S.; George, S. M.; George, S. M.; Jung, Y. S.; Lee, S.-H.; Dillon, A. C. Conformal Surface Coatings To Enable High Volume Expansion Li-Ion Anode Materials. *ChemPhysChem* **2010**, *11*, 2124–2130.
27. Lee, J.-T.; Wang, F.-M.; Cheng, C.-S.; Li, C.-C.; Lin, C.-H. Low-Temperature Atomic Layer Deposited Al_2O_3 Thin Film on Layer Structure Cathode for Enhanced Cycleability in Lithium-Ion Batteries. *Electrochim. Acta* **2010**, *55*, 4002–4006.
28. Atta, S. V.; Cavanagh, A. S.; George, S. M.; Liu, P.; Dillon, A. C.; Lee, S.-H. Electrochemical Effects of ALD Surface Modification on Combustion Synthesized $LiNi_{1/3}Mn_{1/3}Co_{1/3}O_2$ as a Layered-Cathode Material. *J. Power Sources* **2011**, *196*, 3317–3324.
29. Kim, H.; Lee, J. T.; Lee, D.-C.; Magasinski, A.; Cho, W.-I.; Yushin, G. Plasma-Enhanced Atomic Layer Deposition of Ultrathin Oxide Coatings for Stabilized Lithium–Sulfur Batteries. *Adv. Energy Mater.* **2013**, *3*, 1308–1315.
30. Jung, S. C.; Han, Y.-K. How Do Li Atoms Pass through the Al_2O_3 Coating Layer during Lithiation in Li-Ion Batteries? *J. Phys. Chem. Lett.* **2013**, *4*, 2681–2685.
31. Aurbach, D.; Talyosef, Y.; Markovsky, B.; Markevich, E.; Zinigrad, E.; Asraf, L.; Gnanaraj, J. S.; Kim, H.-J. Design of Electrolyte Solutions for Li and Li-Ion Batteries: A Review. *Electrochim. Acta* **2004**, *50*, 247–254.
32. Peng, Z.; Freunberger, S. A.; Chen, Y.; Bruce, P. G. A Reversible and Higher-Rate Li-O_2 Battery. *Science* **2012**, *337*, 563–566.
33. Holzapfel, M.; Wuersig, A.; Scheifele, W.; Vetter, J.; Novak, P. Oxygen, Hydrogen, Ethylene and CO_2 Development in Lithium-Ion Batteries. *J. Power Sources* **2007**, *174*, 1156–1160.
34. Bieker, G.; Bieker, P. M.; Winter, M. Electrochemical *In Situ* Investigations of the SEI and Dendrite Formation on the Lithium Metal Anode. *Phys. Chem. Chem. Phys.* **2015**, 1–13.
35. Han, X.; Xu, Y.; Chen, X.; Chen, Y.-C.; Weadock, N.; Wan, J.; Zhu, H.; Liu, Y.; Li, H.; Rubloff, G.; et al. Reactivation of Dissolved Polysulfides in Li–S Batteries Based on Atomic Layer Deposition of Al. *Nano Energy* **2013**, 1–10.
36. Zhou, G.; Zhao, Y.; Manthiram, A. Dual Confined Flexible Sulfur Cathodes Encapsulated in Nitrogen Doped Double Shelled Hollow Carbon Spheres and Wrapped with Graphene for Li–S Batteries. *Adv. Energy Mater.* **2015**, 1402263–1402273.
37. Elazari, R.; Salitra, G.; Garsuch, A.; Panchenko, A.; Aurbach, D. Sulfur-Impregnated Activated Carbon Fiber Cloth as a Binder-Free Cathode for Rechargeable Li-S Batteries. *Adv. Mater.* **2011**, *23*, 5641–5644.
38. Ryu, H.; Ahn, H.; Kim, K.; Ahn, J.; Lee, J.; Cairns, E. Self-Discharge of Lithium–Sulfur Cells Using Stainless-Steel Current-Collectors. *J. Power Sources* **2005**, *140*, 365–369.
39. Leung, K. Electronic Structure Modeling of Electrochemical Reactions at Electrode/Electrolyte Interfaces in Lithium Ion Batteries. *J. Phys. Chem. C* **2013**, *117*, 1539–1547.
40. Leung, K.; Qi, Y.; Zavadil, K. R.; Dillon, A. C.; Cavanagh, A. S.; Lee, S.-H.; George, S. M. Using Atomic Layer Deposition to Hinder Solvent Decomposition in Lithium Ion Batteries: First-Principles Modeling and Experimental Studies. *J. Am. Chem. Soc.* **2011**, *133*, 14741–14754.
41. Kessels, E.; Putkonen, M. Advanced Process Technologies: Plasma, Direct-Write, Atmospheric Pressure, and Roll-to-Roll ALD. *MRS Bull.* **2011**, *36*, 907–913.